13.5 years of Gravity Waves over Antarctica derived using Interleaved Data Processing Methods: Baselines and Variations

Jackson Jandreau and Xinzhao Chu, *CIRES, CU Boulder*

Introduction

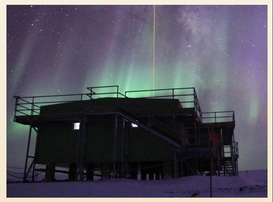

Above: Arrival Heights lidar facility showing the Na Doppler beam

Observations of atmospheric gravity waves (GW) have been made at McMurdo (McM) Station, Antarctica since 2010. Lidar's high-resolution allows observation of the entire GW spectrum.

GW play a key role in upper atmo. energy budget:
- Major method of vertical energy transportation
- Primary driver for mesospheric zonal flow
- Impact the ionospheric by driving TIDs

Unique properties of GW observed by McMurdo lidar:
- Persistent, present in every observation
- Different properties in middle vs. upper atmosphere
- Extend into the thermosphere, visible in Na-layers

New developments in GW research require a full analysis of their behavior in the McMurdo data:
- New techniques improve observation accuracy
- Secondary waves and multistep vertical coupling
- Contribution of unbroken waves to atmo. mixing

Newly Developed Techniques Eliminate Biases and Noise Floors

Second-order parameters like power spectra and variance inherently contain a bias caused by noise in the photon detection process.

Gardner and Chu (2020) developed the interleaved method for removing variance bias by instead using the covariance of two samples.

Interleaving turns a single sample into two, same-volume samples with no shared noise.

Uncorrelated terms drop upon averaging, eliminating biases. Jandreau and Chu (2022) explored this method further.

(Signal, Mean-Zero Noise, Bias)

$$T = T_{bkg} + T'_{Waves} + T'_{Noise} \qquad T' = T'_{Wave} + T'_{Noise}$$

$$Var(T') = \overline{(T'_{Wave})^2} + \overline{2T'_{Wave}T'_{Noise}} + \overline{(T'_{Noise})^2}$$

$$Cov(T'_A, T'_B) = \overline{T'_{A,Wave} * T'_{B,Wave}} + \overline{T'_{A,Wave}T'_{B,Noise}} + \overline{T'_{A,Wave}T'_{B,Noise}} + \overline{T'_{A,Noise} * T'_{B,Noise}}$$

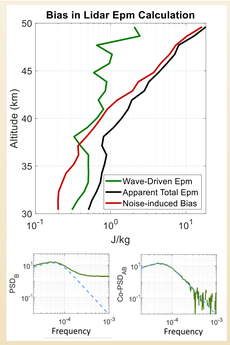

Above: Lidar data noise-variance bias (top) and modeled noise floor
Below: Epm derived without removing noise-variance bias (Lu et al. 2015)

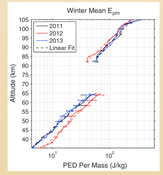

Application to Data

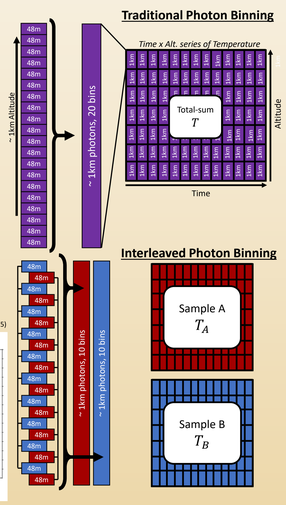

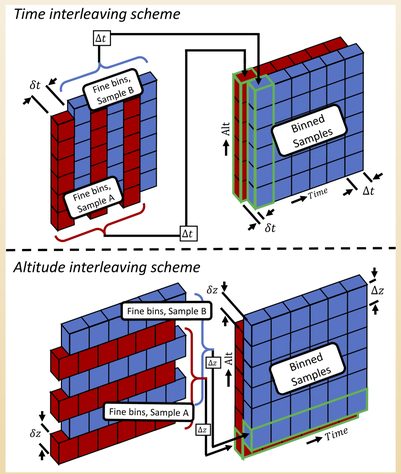

Spectral Interleaving

Gardner and Chu (2020) suggest using the interleaved method for deriving power spectra that inherently have no noise floor. They provide the following equation: $F_{T'}(\omega) \simeq \left|\overline{DFT_\omega(T'_A)DFT^*_\omega(T'_B)}\right|$

This approach of taking the absolute magnitude of the Cross-power Spectral Density, $|CPSD|$, reflects the calculation of $PSD = |DFT|^2$. Alternatively, one can use Co-PSD, the real part of CPSD: $Co{-}PSD = Re(CPSD)$, as seen below:

Anatomy of Interleaved Spectral terms:

$$CPSD = \overline{CPSD_{inst}} = Co + \Delta Co + i(Q + \Delta Q)$$

$$|CPSD| = \sqrt{(Co + \Delta Co)^2 + (Q + \Delta Q)^2} =$$

$$\sqrt{Co^2 + Q^2 + 2Co\Delta Co + 2Q\Delta Q + (\Delta Co)^2 + (\Delta Q)^2}$$

$$Co{-}PSD = Re(CPSD) = Co + \Delta Co$$

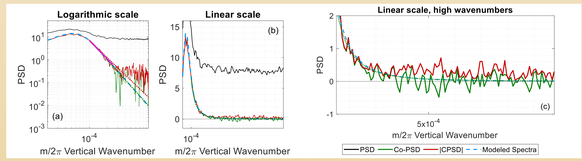

Gravity Wave Energy and Spectra Baselines

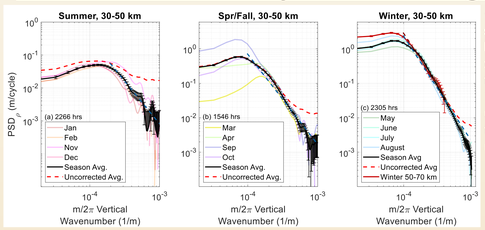

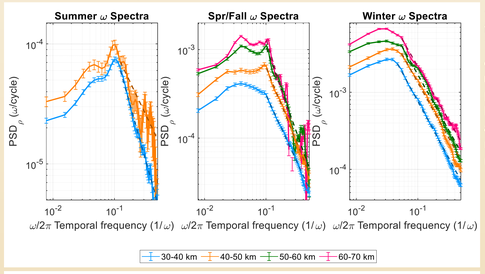

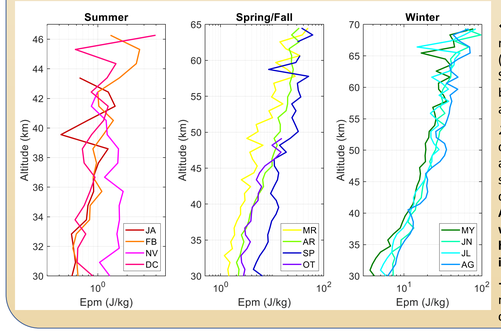

← **The vertical wavenumber spectra show the expected -3 slope in the linear region and show no obvious m^* trend.** These will be compared with the magnitudes predicted by theory. Plotted atop these averages is the uncorrected average, to demonstrate the effect of the spectral interleaved method at removing the noise floor.

m-Spectra slopes

Season \ Altitude	30-50 km	50-70 km
Summer	-2.33* ± 0.16	
Spr/Fall	-2.58 ± 0.03	
Winter	-2.97 ± 0.03	-3.75 ± 0.07

← These temporal spectra reflect those previously derived from McMurdo, showing a slight increase in ω^* with altitude. **Slopes of the linear regions are approximately -5/3** as predicted by linear saturation theory but show a slight steepening with altitude. Higher altitudes also have more noise, so additional work is needed to confirm this effect is real.

ω-Spectra slopes

Alt/ season	30-40 km	40-50 km	50-60 km	60-70 km
Summer	-1.82 ± 0.06	-1.07 ± 0.17		
Spr/Fall	-1.51 ± 0.03	-1.70 ± 0.04	-1.95 ± 0.12	-2.32 ± 0.5
Winter	-1.47 ± 0.02	-1.43 ± 0.03	-1.44 ± 0.01	-1.39 ± 0.01

← While summer and winter are relatively similar from month to month (November as the main difference), Spring/Fall show clear differences between March and April in magnitude and scale height.

↗ Side-by-side, the Epm seasonal difference is clear as well. The adiabatic growth rate is plotted as a solid line, showing the difference in dissipation of each season. **Additionally, the lower half of the winter Epm shows a different scale height than the top (~11.5 vs ~24 km), implying some change in dissipation.**

→ While MLT Epm is preliminary, these new winter results show a more continuous growth between regions.

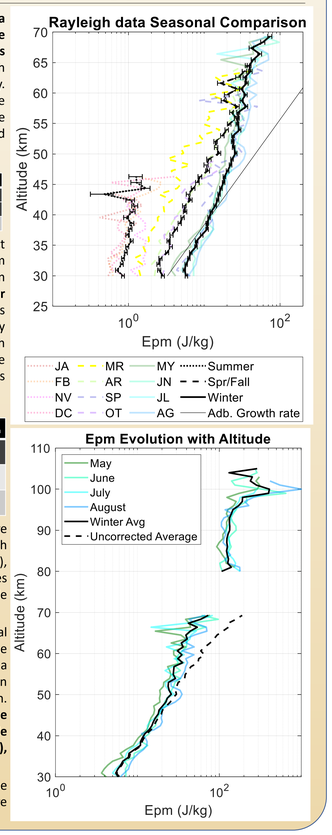

Equatorial-Polar Coupling, 13.5 years of Observation

Li et al. (2020) found correlation between 2011-2019 gravity wave energy over McMurdo, the southern polar vortex width, and the equatorial Quasibiennial Oscillation (QBO) phase.

- **Easterly QBO** phases corresponded to **higher wintertime GW energy** from 30-50 km
- No relation to the El Nino Southern Oscillation (ENSO) was found, though 2011-19 is only ~1.5 ENSO cycles

This investigation revealed new discoveries:
- **The QBO phase modulates the polar vortex width (see figure on right)**
- **Vortex & PNJ move equatorially during easterly QBO phase (see figure on right)**
- **QBO modulates wave filtering, governing gravity wave energy vertical propagation**

Remaining work:
- Find confident ENSO correlations (use more data)
- Determine mechanism linking QBO & Vortex

Additional lidar data from 2020 and 2022-2024 and the Epm derived via the Interleaved method allow the extension of this study, possibly revealing new correlations, see below:

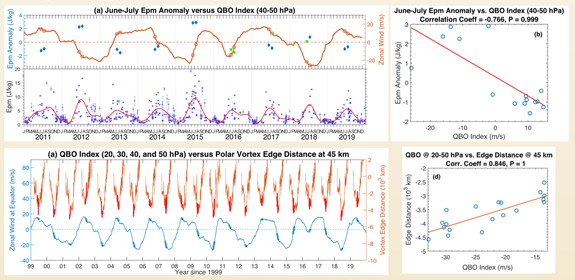

Above: Epm and Vortex position correlations with QBO phase (Li et al. 2020)

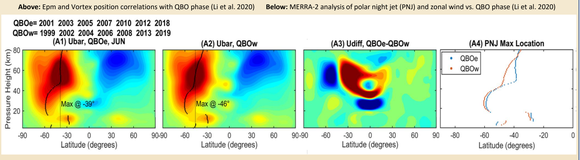

Below: MERRA-2 analysis of polar night jet (PNJ) and zonal wind vs. QBO phase (Li et al. 2020)

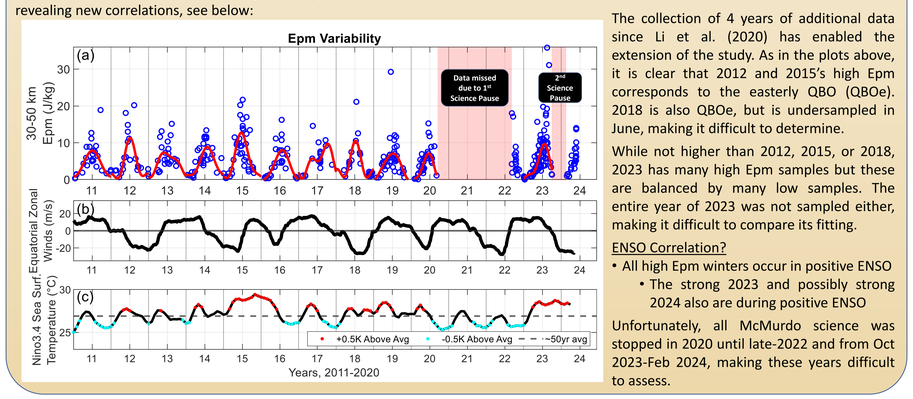

The collection of 4 years of additional data since Li et al. (2020) has enabled the extension of the study. As in the plots above, it is clear that 2012 and 2015's high Epm corresponds to the easterly QBO (QBOe). 2018 is also QBOe, but is undersampled in June, making it difficult to determine.

While not higher than 2012, 2015, or 2018, 2023 has many high Epm samples but these are balanced by many low samples. The entire year of 2023 was not sampled either, making it difficult to compare its fitting.

ENSO Correlation?
- All high Epm winters occur in positive ENSO
  - The strong 2023 and possibly strong 2024 also are during positive ENSO

Unfortunately, all McMurdo science was stopped in 2020 until late-2022 and from Oct 2023-Feb 2024, making these years difficult to assess.

Major Points and Next Steps

Interleaved Methods:
- The interleaved method has increased the range of altitudes and extent of low-SNR in which GWs can be reliably analyzed
- There are other applications as well, such as determining a more accurate ratio of upwards/downwards waves
- **Spatial interleaving can be done with satellite imagers, like Atmospheric Wave Experiment (AWE) airglow observations**

Energy:
- Larger scale heights in 50-70 km winter GW Epm imply stronger dissipative processes or wave breaking in this region
- While MLT Epm is preliminary, interleaved Epm shows a new picture of stratosphere/mesosphere to MLT wave growth

Spectra
- Using new methods, spectra are observed which match theory and past observations. Comparison with magnitudes will be conducted
- Seasonal trends in slope are observed for the first time which will be further analyzed for mechanism and validity

Interannual Variations
- Possible ENSO correlations are observed in new data, further study is needed. **Months of lost data makes this comparison difficult**

Key References

Chen, C., Chu, X., McDonald, A. J., Vadas, S. L., Yu, Z., Fong, W., & Lu, X. (2013). Inertia-gravity waves in Antarctica: A case study using simultaneous lidar and radar measurements at McMurdo/Scott Base (77.8°S, 166.7°E). *Journal of Geophysical Research: Atmospheres*, *118*(7), 2794–2808. https://doi.org/10.1002/jgrd.50318

Chen, C., Chu, X., Zhao, J., Roberts, B. R., Yu, Z., Fong, W., Lu, X., & Smith, J. A. (2016). Lidar observations of persistent gravity waves with periods of 3–10h in the Antarctic middle and upper atmosphere at McMurdo (77.83°S, 166.67°E). *Journal of Geophysical Research: Space Physics*, *121*(2), 1483–1502. https://doi.org/10.1002/2015JA022127

Chu, X., Huang, W., Fong, W., Yu, Z., Wang, Z., Smith, J. A., & Gardner, C. S. (2011). First lidar observations of polar mesospheric clouds and Fe temperatures at McMurdo (77.8°S,166.7°E), Antarctica. *Geophysical Research Letters*, *38*, L16810. https://doi.org/10.1029/2011GL048373

Chu, X., Yu, Z., Gardner, C. S., Chen, C., & Fong, W. (2011). Lidar observations of neutral Fe layers and fast gravity waves in the thermosphere (110-155 km) at McMurdo (77.8°S,166.7°E), Antarctica. *Geophysical Research Letters*, *38*, L23807. https://doi.org/10.1029/2011GL050016

Chu, X., Zhao, J., Lu, X., Harvey, V. L., Jones, R. M., Becker, E., Chen, C., Fong, W., Yu, Z., Roberts, B. R., & Dörnbrack, A. (2018). Lidar Observations of Stratospheric Gravity Waves From 2011 to 2015 at McMurdo (77.84°S, 166.69°E), Antarctica: 2. Potential Energy Densities, Lognormal Distributions, and Seasonal Variations. *Journal of Geophysical Research: Atmospheres*, *123*(15), 7910–7934. https://doi.org/10.1029/2017JD027386

Gardner, C. S. (2018). Role of Wave-Induced Diffusion and Energy Flux in the Vertical Transport of Atmospheric Constituents in the Mesopause Region. *Journal of Geophysical Research: Atmospheres*, *123*(12), 6581–6604. https://doi.org/10.1029/2018JD028359

Gardner, C. S., & Chu, X. (2020). Eliminating photon noise biases in the computation of second-order statistics of lidar temperature, wind, and species measurements. *Applied Optics*, *59*(27), 8259–8271. https://doi.org/10.1364/AO.400375

Lu, X., Chu, X., Fong, W., Chen, C., Yu, Z., Roberts, B. R., & McDonald, A. J. (2015). Vertical evolution of potential energy density and vertical wave number spectrum of Antarctic gravity waves from 35 to 105 km at McMurdo (77.8°S, 166.7°E): GW Energy Density and Wavenumber Spectra. *Journal of Geophysical Research: Atmospheres*, *120*(7), 2719–2737. https://doi.org/10.1002/2014JD022751

Vadas, S. L. (2013). Compressible *f* -plane solutions to body forces, heatings, and coolings, and application to the primary and secondary gravity waves generated by a deep convective plume: COMPRESSIBLE *f* -PLANE SOLUTIONS. *Journal of Geophysical Research: Space Physics*, *118*(5), 2377–2397. https://doi.org/10.1002/jgra.50163

Vadas, S. L., Fritts, D. C., & Alexander, M. J. (2003). Mechanism for the Generation of Secondary Waves in Wave Breaking Regions. *Journal of the Atmospheric Sciences*, *60*(1), 194–214. https://doi.org/10.1175/1520-0469(2003)060<0194:MFTGOS>2.0.CO;2

Vadas, S. L., Zhao, J., Chu, X., & Becker, E. (2018). The Excitation of Secondary Gravity Waves From Local Body Forces: Theory and Observation. *Journal of Geophysical Research: Atmospheres*, *123*(17), 9296–9325. https://doi.org/10.1029/2017JD027270

Zhao, J., Chu, X., Chen, C., Lu, X., Fong, W., Yu, Z., Michael Jones, R., Roberts, B. R., & Dörnbrack, A. (2017). Lidar observations of stratospheric gravity waves from 2011 to 2015 at McMurdo (77.84°S, 166.69°E), Antarctica: 1. Vertical wavelengths, periods, and frequency and vertical wave number spectra. *Journal of Geophysical Research: Atmospheres*, *122*(10), 5041–5062. https://doi.org/10.1002/2016JD026368

McMurdo lidar projects are supported by NSF Grants OPP-2110428, Jackson is partially supported by NASA 80NSSC22K1854